

Coupling between Global Geometry and the Local Hall Effect Leading to Reconnection-Layer Symmetry Breaking

Michiaki Inomoto,^{*} Stefan P. Gerhardt, Masaaki Yamada, Hantao Ji, Elena Belova, Aleksey Kuritsyn,[†] and Yang Ren

Center for Magnetic Self-Organization in Laboratory and Astrophysical Plasmas, Princeton Plasma Physics Laboratory, Princeton University, Princeton, New Jersey 08543, USA

(Received 29 March 2006; published 27 September 2006)

The coupling between the global reconnection geometry and the local microphysics, caused by the Hall effect, is studied during counterhelicity plasma merging in the magnetic reconnection experiment. The structure of the reconnection layer is significantly modified by reversing the sign of the toroidal fields, which affects the manifestation of the Hall effect in the collisionless regime. The local two-fluids physics changes the global boundary conditions, and this combination effect consequently provides different reconnection rates, magnetic field structure, and plasma flow patterns for two different counterhelicity merging cases in the collisionless regime.

DOI: [10.1103/PhysRevLett.97.135002](https://doi.org/10.1103/PhysRevLett.97.135002)

PACS numbers: 52.35.Vd, 52.72.+v

Magnetic reconnection [1], the breaking of the frozen-in condition of magnetic field lines in electrically conducting plasmas, plays an important role in global magnetic self-organization phenomena in laboratory and space plasmas. It has been recognized that the reconnection rate is determined by both local microphysics mechanisms and the global boundary conditions [2]. Local microphysics emerges when the scale lengths become shorter than the ion inertial length. Within the electron inertial region, the electron frozen-in condition is broken by electron inertia or the off-diagonal components of the pressure tensor [3–5]. Within an ion inertial region but outside the electron inertial region, a separation of the demagnetized ion and magnetized electron motion occurs. This leads to the Hall effect [6–16], one of the key mechanisms which contributes to the fast reconnection rate in collisionless regime. The quadrupole out-of-plane field, clear evidence of the Hall effect, is observed during the null-helicity “pull” reconnection experiments in the magnetic reconnection experiment (MRX) [6,7].

In this Letter, we report that symmetry breaking of the magnetic reconnection layer due to local two-fluid physics, the Hall effect, is observed in MRX. The plasma flows and magnetic reconnection rates are significantly modified through an interaction between the local Hall effect and global boundary conditions. The observation is made through the different radial shifts of the neutral sheet X line during two types of counterhelicity merging [17–19], that is, plasma merging of two spheromaks with opposite toroidal fields. This X -line motion splits the counterhelicity merging into two different states: one case with a radially pushed-in X line and the other case with a radially pushed-out X line, depending on the sign of the toroidal magnetic fields of two merging plasmas. The bifurcated counterhelicity states, which cannot be explained within the MHD framework, result in different magnetic field structures and reconnection rates due to the local two-fluid

physics and the associated changes of the global boundary conditions of reconnection. These effects are strongest in the collisionless regime, as expected for Hall physics. Given that the local microphysics and the global boundary conditions can both determine the reconnection rate, a significant finding of the present results is that the local two-fluid reconnection physics modifies the global boundary conditions, and their combined effect consequently determines the reconnection rate and magnetic field line structures.

In counterhelicity merging, both poloidal and toroidal magnetic fields reconnect, introducing a unique three-dimensional feature to the magnetic reconnection geometry. Figure 1 shows a schematic cross-sectional view of the MRX vacuum vessel together with the key diagnostics utilized in this research. Two flux cores, containing both poloidally and toroidally wound coils, are used to produce two spheromaks [20]. The spheromaks approach together and then merge into one field-reversed configuration, in

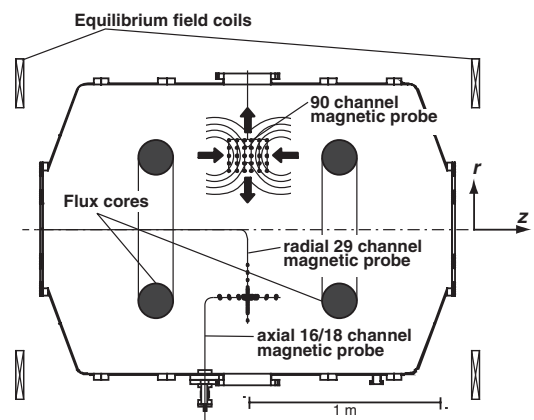


FIG. 1. Schematic view of MRX experimental setup. Arrows indicate plasma inflow and outflow directions to/from the X line in counterhelicity merging experiments.

which toroidal flux is canceled through magnetic reconnection [19,21,22]. A 90 channel array of coil triplets on a 6×5 grid (4 cm spacing) is utilized to measure all three components of the magnetic field in the r - z plane. More fine-scale measurements are made with two linear arrays. The first linear array measures B_z at 29 points along a radial line. The second array, oriented in the axial direction and radially scannable, measures B_r at 16 locations and B_t at 18 locations. Note that the reconnection inflow and outflow in these counterhelicity merging experiments are the z (axial) and r (radial) directions, respectively. These directions are reversed ($r \rightarrow z$ and $z \rightarrow r$) from previous pull reconnection experiments in MRX [6,7]. Steady and reproducible “push” magnetic reconnection is achieved in the early phase of the spheromak merging [17] before the two spheromak plasmas are pinched off from the flux cores and the plasma evolution becomes irreproducible.

Counterhelicity merging has two different states, characterized by sign of the toroidal field of the two initial spheromaks, as shown in Fig. 2(a). We define the case with positive toroidal field in the left-side spheromak and negative toroidal field in the right-side spheromak as “case I” and the case with both toroidal fields reversed as “case O,” where the z axis is taken toward the right. Since both poloidal and toroidal components of the magnetic field lines reconnect in counterhelicity merging, the reconnection plane is tilted with respect to the r - z plane. Furthermore, the reconnection planes of cases I and O are oppositely tilted as shown in Fig. 2(b). These two cases are thus different with regard to the sign of radial component of the reconnection current or electric field. Although this difference does not affect the reconnection process in the MHD regime, a significant difference is observed in the collisionless two-fluid regime, as shown in Fig. 3.

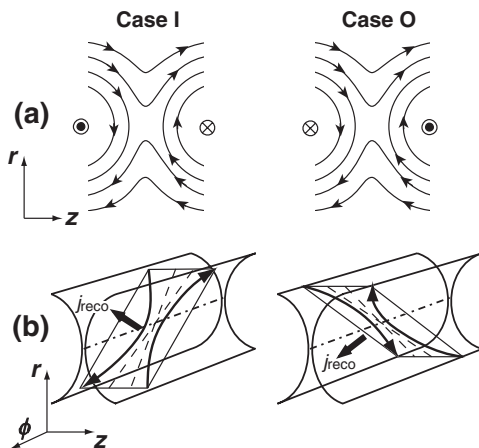


FIG. 2. Two-dimensional (a) and three-dimensional (b) illustrations of reconnecting magnetic field lines in cases I (left) and O (right) counterhelicity merging in the MHD regime. The reconnection current j_{reco} has opposite radial components in cases I and O.

Figures 3(a) and 3(b) show the measured magnetic field structure in counterhelicity merging at $t = 240 \mu\text{s}$ (a) and $t = 260 \mu\text{s}$ (b), as measured by the 90 channel probe array. The arrows indicate the poloidal magnetic field vector (B_r , B_z) and the color code indicates the toroidal magnetic field (B_t). The contour lines of poloidal flux $\Psi(z, r) = \int_0^r 2\pi r' B_z(z, r') dr'$ are shown by black solid lines (spacing is 0.2 mWb). Figure 3(a), measured at $t = 240 \mu\text{s}$, corresponds to the beginning of magnetic reconnection, and the initial radial position of the X line is the same for both cases. Poloidal and toroidal fields accumulate during the initiation of the reconnection process, and the X line is observed to move toward the inboard side in case I [Fig. 3(b), left] or the outboard side in case O [Fig. 3(b), right]. The system then settles into a steady state, with a stationary X point throughout the duration of reconnection.

This symmetry breaking phenomena can be explained by the Hall effect in counterhelicity magnetic reconnection geometry. Figure 3(c) shows three-dimensional illustrations of the reconnecting field line structure in cases I and O in the Hall-MHD regime. In this regime, the ion motion is detached from the electron motion in the vicinity of the X line, generating the “Hall current” in the tilted reconnection plane. This Hall effect produces a quadrupole magnetic field in the null-helicity reconnection case as the reconnecting magnetic fields are pulled by the electron fluid in the direction of the sheet current [8]. In the present counterhelicity merging case, the reconnecting field lines are pulled toward the inboard side in case I [Fig. 3(c), left] since the reconnection current has positive radial component. Case O [Fig. 3(c), right] shows the reverse of case I: the reconnecting field lines are pulled toward the outboard side. The Hall-MHD picture of cases I and O qualitatively

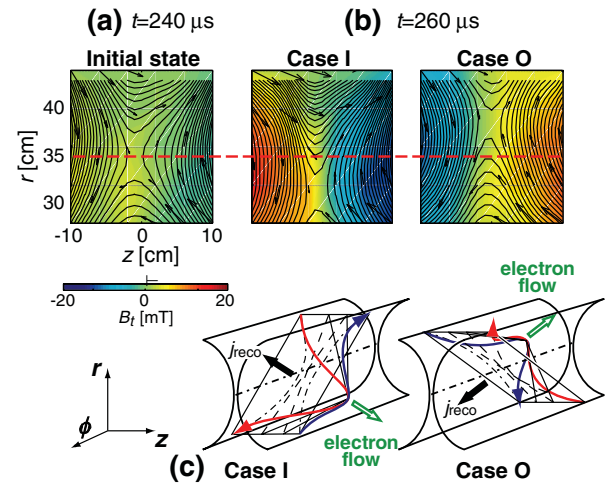


FIG. 3 (color). Measured poloidal magnetic flux contours (solid lines) with poloidal magnetic field (arrows) and toroidal magnetic field (color coded) at $t = 240 \mu\text{s}$ (a) and $t = 260 \mu\text{s}$ (b) in cases I (left) and O (right) counterhelicity merging, and corresponding three-dimensional illustrations of reconnecting field lines in the Hall-MHD regime (c).

agrees with the experimental results shown in Fig. 3(b). Note that the naming convention is now clear: I is for the case with the inward shift, and O is for the case with the outward shift.

The X -line radial motion becomes strong when the plasma is in the collisionless regime, supporting the notion that this motion is caused by the two-fluid Hall effect. Figure 4(a) shows the X -line shift distance from the vacuum null point as a function of collisionality parameter $\delta/\lambda_{\text{mfp}}$, where δ is the current sheet width and λ_{mfp} is the electron mean free path. The shift distance in case I [Fig. 4(a), left] increases gradually as the collisionality parameter is decreased, i.e., as plasma becomes collisionless. A similar but sharper trend appears in case O [Fig. 4(a), right]. Note that cases I and O shown in Fig. 3(b) correspond to the case with collisionality parameter $\delta/\lambda_{\text{mfp}} \sim 6$.

In order to understand the impact of Hall physics on the reconnection rate, consider the electron force balance equation. A generalized Ohm law including the Hall term can be expressed as

$$\mathbf{E} + \mathbf{v} \times \mathbf{B} = \eta \mathbf{j} + \frac{\mathbf{j} \times \mathbf{B}}{en}. \quad (1)$$

At the point far upstream of the X line, the ideal MHD condition of $\mathbf{E} + \mathbf{v} \times \mathbf{B} = \mathbf{0}$ is expected assuming the resistive and the Hall terms are small enough to be neglected outside the diffusion region. At intermediate posi-

tions between the X line and the far upstream position, e.g., the shoulder of the current sheet layer, the Hall and the resistivity terms sustain the large reconnection electric field as $\mathbf{E} = \eta \mathbf{j} + \frac{\mathbf{j} \times \mathbf{B}}{en}$. From the toroidal component of these equations, the plasma inflow velocity toward the diffusion region is approximately expressed as $V_{in} = |\nu_z| = |E_t/B_r| \approx |\eta_{\perp} j_t/B_r + j_z/en|$, where η_{\perp} is the perpendicular Spitzer resistivity, B_r is the reconnecting magnetic field, j_z is the axial current density, and E_t and j_t are the toroidal components of reconnection electric field and current, respectively. Here we assume that the axial magnetic field B_z is negligible in the inflow region. The normalized reconnection rate V_{in}/V_A is expressed in (2), where V_A is the upstream Alfvén velocity:

$$\frac{V_{in}}{V_A} \approx \frac{\eta_{\perp} j_t}{B_r V_A} + \frac{j_z}{en V_A}. \quad (2)$$

Here, the reconnection rate is divided into the resistive diffusion term (the first term of the right-hand side) and the Hall effect term (the second term of the right-hand side).

Figure 4(b) shows the reconnection rate V_{in}/V_A (solid circle), the resistive diffusion term $\eta_{\perp} j_t/(B_r V_A)$ (open triangle), and the Hall effect term $j_z/(en V_A)$ (open square) measured independently as a function of the collisionality parameter $\delta/\lambda_{\text{mfp}}$. The resistive and Hall terms are evaluated at the shoulder of the current sheet. All values are calculated during the quasisteady state after the X -line motion has settled down. The reconnection rate V_{in}/V_A is enhanced in the collisionless regime. However, case O [Fig. 4(b), right] has a reconnection rate that is approximately 50% larger than case I [Fig. 4(b), left] in the collisionless limit.

The resistive term in both cases stays small in the collisionless regime and reaches a value comparable to the reconnection rate in the collisional regime. The Hall term shows a trend which is very similar to the reconnection rate, suggesting that the enhancement of the reconnection rate in the collisionless regime is dominated by the Hall term, although some other microscopic mechanisms, such as anomalous resistivity by turbulence [23] or the effects of off-diagonal components in electron pressure tensor [3–5], are required to explain the breaking of the frozen-in condition inside the electron inertia region where the Hall term vanishes. Nevertheless, the reconnection electric field in the vicinity of the X point is mainly sustained by the Hall term [3]. The next question is this: Why is there a difference between the two cases; that is, why does case O yield a larger Hall term and faster reconnection than case I?

Since the axisymmetric X -line motion takes place for a short duration during the initiation of reconnection, it will invoke a certain compression or expansion of the magnetic field at the inboard or outboard side of the X line, based on the assumption of flux conservation at the X line and the

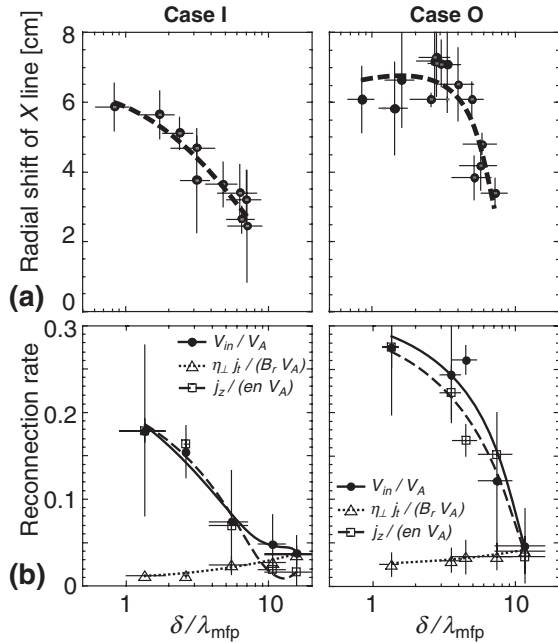


FIG. 4. Radial shift of the X line (a) and total reconnection rate (solid circle), resistive diffusion term (open triangle), and the Hall term (open square) in the generalized Ohm law (b) as functions of collisionality parameter in cases I (left) and O (right) counterhelicity merging. The curves are approximating polynomials.

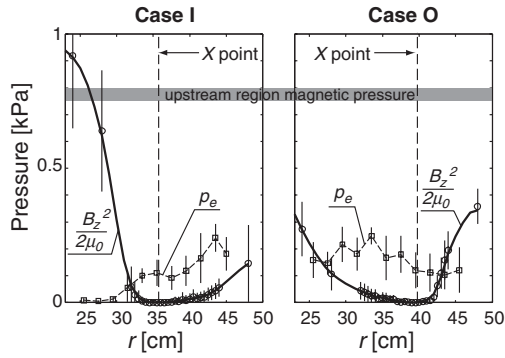


FIG. 5. Radial profiles of axial magnetic field pressure (circles) and electron thermal pressure (squares) measured on the mid-plane ($z = 0$) in cases I (left) and O (right) counterhelicity merging.

chamber wall. Radial profiles of the magnetic field pressure during counterhelicity merging in the very collisionless regime ($\delta/\lambda_{\text{mfp}} \sim 1$) are shown in Fig. 5, together with electron thermal pressure $p_e = kn_e T_e$ measured by a triple Langmuir probe on the midplane ($z = 0$). The magnetic field pressure in case I (Fig. 5, left) reaches about 1 kPa at the inboard side of the X line, which is even larger than the magnetic pressure in the upstream region (750–800 Pa), indicated in Fig. 5 by a gray area. Therefore, the reconnection outflow cannot go to the inboard side in case I. This reduced outflow on the inboard side is also suggested by the steep falloff of the electron thermal pressure on the inboard side of the X line. Although case O (Fig. 5, right) shows an increase of magnetic pressure at the outboard side of the X line, it is smaller than the magnetic pressure in the upstream region and bidirectional outflow is expected, as in common two-dimensional reconnection. This difference in magnetic pressure quantitatively agrees with the estimation from X-line shift shown in Fig. 4(a) with assumption of the flux conservation at the X line, and can account for the difference of the reconnection rate shown in Fig. 4(b) because of the different outflows. This phenomenon demonstrates that the local Hall effect can change the global magnetic structure and even the boundary conditions of magnetic reconnection. The microphysics and global boundary conditions are not independent but are coupled through the Hall effect in the present experimental geometry. These results, coupled with previous studies [6–16], indicate that the Hall effect is common in many different reconnection situations but that its manifestations are geometry dependent.

In summary, the Hall effect yields an X-line radial shift in the collisionless counterhelicity merging. This X-line shift, which is due to the same physics as the well-known quadrupole out-of-plane magnetic field, leads to two differentiated states of counterhelicity merging with different

magnetic field structure, pressure profiles, and reconnection rates. Hence, we observe symmetry breaking of the system due to the combined behavior of the Hall effect and the associated global boundary conditions. The local two-fluid effect modifies the global reconnection phenomena and the global boundary conditions affect the local reconnection mechanisms, as clearly observed in those collisionless counterhelicity merging experiments. We find a vivid example about how local dynamics and the global boundary conditions interact with each other to determine the self-consistent process of magnetic reconnection.

The authors would like to thank Professor R. Kulsrud and Professor Y. Ono for fruitful discussion, and Mr. R. Cutler and Mr. D. Cylinder for skillful technical support. This work was supported by MEXT-Japan, U.S. DOE, NASA, and NSF.

*Permanent address: Osaka University, Osaka 565-0871, Japan.

†Permanent address: The University of Wisconsin—Madison, Madison, WI 53706, USA.

- [1] D. Biskamp, *Magnetic Reconnection in Plasmas* (Cambridge University Press, Cambridge, UK, 2000); E. Priest and T. Forbes, *Magnetic Reconnection* (Cambridge University Press, Cambridge, UK, 2000).
- [2] H. Ji *et al.*, Phys. Plasmas **6**, 1743 (1999).
- [3] L. Yin and D. Winske, Phys. Plasmas **10**, 1595 (2003).
- [4] C.H. Jaroschek *et al.*, Phys. Plasmas **11**, 1151 (2004).
- [5] N. Bessho and A. Bhattacharjee, Phys. Rev. Lett. **95**, 245001 (2005).
- [6] Y. Ren *et al.*, Phys. Rev. Lett. **95**, 055003 (2005).
- [7] M. Yamada *et al.*, Phys. Plasmas **13**, 052119 (2006).
- [8] M.E. Mandt, R.E. Denton, and J.F. Drake, Geophys. Res. Lett. **21**, 73 (1994).
- [9] D. Biskamp, E. Schwarz, and J.F. Drake, Phys. Rev. Lett. **75**, 3850 (1995).
- [10] M.A. Shay *et al.*, J. Geophys. Res. **106**, 3759 (2001).
- [11] P.L. Pritchett, J. Geophys. Res. **106**, 3783 (2001).
- [12] M. Øieroset *et al.*, Nature (London) **412**, 414 (2001).
- [13] T. Nagai *et al.*, J. Geophys. Res. **106**, 25929 (2001).
- [14] F.S. Mozer, S.D. Bale, and T.D. Phan, Phys. Rev. Lett. **89**, 015002 (2002).
- [15] A. Vaivads *et al.*, Phys. Rev. Lett. **93**, 105001 (2004).
- [16] W.H. Matthaeus *et al.*, Geophys. Res. Lett. **32**, L23104 (2005).
- [17] M. Yamada *et al.*, Phys. Plasmas **4**, 1936 (1997).
- [18] M. Yamada *et al.*, Phys. Rev. Lett. **65**, 721 (1990).
- [19] Y. Ono *et al.*, Phys. Rev. Lett. **76**, 3328 (1996).
- [20] M. Yamada *et al.*, Phys. Rev. Lett. **46**, 188 (1981).
- [21] T.-H. Watanabe, T. Sato, and T. Hayashi, Phys. Plasmas **4**, 1297 (1997).
- [22] C.D. Cothran *et al.*, Phys. Plasmas **10**, 1748 (2003).
- [23] H. Ji *et al.*, Phys. Rev. Lett. **92**, 115001 (2004).